WEAT Report No. 18

UNIVERSITY OF OKLAHOMA OFFICE OF RESEARCH ADMINISTRATION

ATMOSPHERIC RESEARCH LABORATORY

Norman, Oklahoma

RECTIFICATION OF A WHOLE-SKY PHOTOGRAPH AS A TOOL FOR DETERMINING SPATIAL POSITIONING OF CUMULUS CLOUDS

by

BOB E. STUCKY

This research was supported

by

National Aeronautics and Space Administration

Research Grant

NAS 9-13360

April, 1975

UNIVERSITY OF OKLAHOMA OFFICE OF RESEARCH ADMINISTRATION

ATMOSPHERIC RESEARCH LABORATORY

Norman, Oklahoma

RECTIFICATION OF A WHOLE-SKY PHOTOGRAPH AS A TOOL FOR DETERMINING SPATIAL POSITIONING OF CUMULUS CLOUDS

by

BOB E. STUCKY

This research was supported

by

National Aeronautics and Space Administration

Research Grant

NAS 9-13360

April, 1975

ABSTRACT

Whole-sky photographs were taken from Lake Altus, Oklahoma, 11 June 1973, during the approximate pass-time of SKYLAB-2. The base dimensions of selected cumuli and their spacing relative to the camera were determined from a single whole-sky photograph. The individual cumuli were mapped onto an enlarged positive print selected from SKYLAB-2, S190a Color IR film, which was used as reference. Comparisons were made of the cumuli distributions for the two differing photographs, and an attempt to identify the individual cumuli from the whole-sky photo with those corresponding to the S190a enlargement was made. User's errors and utilization of whole-sky photographs and related meteorological studies are commented upon as a direct by-product of the single case study.

RECTIFICATION OF A WHOLE-SKY PHOTOGRAPH AS A TOOL FOR DETERMINING SPATIAL POSITIONING OF CUMULUS CLOUDS

Introduction

The purpose of this note is to investigate the whole-sky photograph as a reliable instrument for determining real-space positioning of cumulus clouds. Once reliability of spatial positioning is established, the whole-sky photographs may become a valuable asset to squall-line dynamical studies, boundary layer theory, and other related phenomena.

Lund and Shanklin (1972 and 1973) utilized the whole-sky photograph for estimating probabilities of cloud-free lines-of-sight (CFLOS) through the atmosphere as a function of zenith angles and sky coverage (coverage in tenths as reported by the National Weather Service). Lund (1973) developed a model for estimating joint probabilities of CFLOS for a station network, and developed the persistence and recurrence probabilities of CFLOS. Rapp, Schultz, and Rodriques (1973) developed a CFLOS probability model as a function of the slant range of clouds by suitably combining the 3-hour synoptic report (cloud height and coverage reported in eighths) and the photographically-derived probability of CFLOS. Krider (1974) studied the propagation of cloud-to-cloud lightning by using extended time-exposures of whole-sky photographs.

As seen from the above, most meteorological applications of the whole-sky photograph has been geared towards determination of

CFLOS and its associated probabilities. Outstanding work by the aforementioned authors and their perception of the important discrepancy between a ground observer's report of sky coverage and a CFLOS certainly deserve merit. However, the ability of the fish-eye lens to provide total sky coverage allows applicability to other related meteorological areas as well.

It must be emphasized that this report considers a single case study in attempting to spatially position cumulus clouds.

Type of Equipment Used

A Nikon Model F camera (35 mm) with a 180° fish-eye lens (Fish-eye-NIKKOR Auto Lens) was used to photograph the whole sky. The lens has an 8 mm focal length, an effective picture-field diameter of 23 mm, and an aperture scale of f/2.8 to f/22. It has a 5-filter capacity and a focusing range of 0.3 m to ∞ (infinity).

The utilization of a wide-angle lens presents an important problem concerning the relationship of the image position on the photo negative relative to its real space location. The problem is one of determining the image-distance zenith-angle properties of the whole-sky photograph.

The type of fish-eye lens used is suitable for adapting to the equidistant projection

$$y = C\,\theta$$

where y is the distance of the object point to the negative's center, C a constant, and θ the zenith angle of the object in question (Fig. 1). Most users of the fish-eye lens apply this linear relationship where C is a property for the type of lens used. For the

type of lens used here, the constant C is approximately 0.14 (mm/deg).

However, for the single case study given here, a nonlinear image-distance zenith-angle relationship was employed as shown in Fig. 2. This nonlinear constraint (given by the operators manual) is suggested due to the nature of the cumuli distribution. Nearly all of the well-defined cumuli bases were located in the lower 30° elevation angles, thus influencing the use of the nonlinear relationship.

A graphical comparison of the linear and nonlinear methods is shown in Fig. 2. Deviations between the two methods begin near the 45° zenith angle and increase for angles greater than 45°. For example, the leading edge of a cloud base positioned 10 mm from the negative center results in nearly a 4° zenith angle difference between the two projections. This 4° deviation produces a corresponding 0.4 km difference (relative to the camera) in the ground projection for the same cloud base (assuming a cloud base altitude of 335 m). For zenith angles $> 45°$, differences in surface projections increase as the base altitude of a given cloud system increases. Thus, the linear assumption can produce substantial errors when attempting to spatially locate elevated objects in the lower 30° elevation angles, especially in the lower 10-15° range.

The type of film used was Kodak 135 color negative film (ASA 25) exposed through the skylight filter (L1A). A sun shield was not used resulting in some loss of color contrast due to the presence of high thin cirrus scattering the incoming solar radiation.

Data Collection Procedure

On 11 June 1973, whole-sky photographs were taken from a small watercraft on Lake Altus, Oklahoma (99°17'W, 35°55'N) during the approximate pass-time of SKYLAB-2 (DOY 162, Pass 8, Ground Track 48). The camera was set with an aperture of f/8, an exposure time of 1/125 sec., and a fixed focus (∞).

A selected whole-sky color negative was enlarged to fit an 8 x 10 photo print. The resultant circular positive print had a diameter of 20.6 cm with a negative enlargement of 8.96 X.

A plastic transparency containing 10° increments of azimuth and zenith angles was fitted to the circular print. The diameter of the transparency was such that the 90° zenith angle circumscribed the outermost diameter of the circular positive print. An example of the plastic template used is shown in Fig. 3.

True north was determined on the whole-sky photo by application of solar azimuth and elevation angles and by proper alignment of small mountain peaks surrounding the lake. Once true north was established, the transparency when placed over the photographs enabled the calculations of base size and relative distances from the camera of the selected cumuli by measuring their zenith and azimuth angles.

Frame 15-31 of the S190a (Multispectural Photographic Facility) Color Positive IR (0.50 to 0.88 μm) film (70 mm) taken from SKYLAB-2, Pass 8 (1518:30 GMT) was used as reference for the whole-sky photograph. The highly sensitive S190a photographic system and its high resolution (30 meter class) allowed an enlargement to 40 X of the Lake Altus area without significant loss in resolution. The

resulting scale of the 40 X enlargement was 1:71500. The whole-sky photograph taken closest in time to the SKYLAB pass-time was selected for the single case study.

There was a 16 km displacement between the center of Frame 15-31 and the origin of the whole-sky coordinate system. This discrepancy was presumed negligible as the altitude (439.25 km) of SKYLAB-2 above the oblate earth was nearly 28 times larger than the 16 km displacement of the whole-sky camera. Thus, the whole-sky origin as viewed from the space platform resulted in an angular displacement of only 2° from nadir, so any cloud distortion over the Lake Altus area was neglected on the enlargement.

Two immediate problems were encountered: the whole-sky photograph center did not represent true zenith and the exposure time of the whole-sky negative was 1520 GMT resulting in a 90 second lag from the SKYLAB-2 pass-time (1518:30 GMT). The former was corrected by closely fitting the arc of the 90° zenith angle from the superimposed transparency to the land-water boundary (only a small adjustment was necessary). The latter was adjusted by translation of the fish-eye coordinate system (on the 40 X enlargement) at a velocity vector equal to the mean wind at an altitude of 335 meters, with a magnitude of 9 m/sec from 200°. Upper air soundings taken during the approximate pass-time of SKYLAB-2 and hourly surface reports were used to determine the altitude of the cumuli bases (near 335 meters) and the winds at cloud base level.

The selected individual cumuli with their respective base size and relative distance from the camera (as determined from the whole-sky photo) were then mapped onto the S190a 40 X enlargement and

comparisons between the two cloud distributions were made.

Analysis

The comparison between the whole-sky photograph and the S190a enlargement was not as satisfactory as was originally anticipated. Fig. 4 displays the two photographically compared cumuli distributions, a result of mapping the pre-determined cloud base dimensions from the whole-sky photograph onto the enlarged S190a print (hatched areas represent selected cumuli from the whole-sky photograph). As shown in Fig. 4, the adjusted position of the camera's coordinates is due to the 90 second time differential, resulting in a 0.81 km displacement from its original location. As can be seen, pattern similarity between the two distributions is poor.

The apparent failure to identify the same cloud base on the two differing photographs is primarily due to three major types of errors:

1) Inaccuracy of the subjectively determined cloud base heights and locations.
2) The employment of a non-synchronized timing system.
3) Rapid formation and dissipation of individual cumuli that can occur during time intervals of 1-5 minutes.

The cloud bases were assumed to have rectangular images on the whole-sky print which should have produced only minor effects upon total analysis error. It was further assumed that errors due to estimating cloud base elevations (335 m) and the mean wind (9 m/sec from 200°) at cloud base level were insignificant to the final analysis.

Lack of a synchronized timing system appears to account for a

major portion of the total analysis error. This deficiency required the translation of whole-sky coordinate system, thus introducing additional errors associated with rapid formation and dissipation of individual cumulus clouds during the 90 second time differential. Application of the 90 second advection time, however, resulted in a poor identification pattern as indicated in Fig. 4. It is suggested that either the 90 second time difference was in error or that rapid cumulus formation and dissipation did occur during the given time lag. It is possible that both conditions existed simultaneously, thereby magnifying analysis errors.

By questioning the reliability of the time (1520 GMT) of whole-sky exposure, a visual trial-and-error technique was attempted by which the whole-sky coordinate system was re-adjusted to different locations on the S190a photo until a better cloud-to-cloud identification pattern resulted. The re-adjustment was constrained to the general direction of the previously used mean wind (at cloud base level). Fig. 5 displays a better correlated cloud identification pattern.

The newly adjusted position of the fish-eye coordinate system is more than four times the distance of the initial adjusted position. The coordinate location was again downstream from the previously used mean wind. A new translated distance of 3.4 km and advection velocity of 9 m/sec dictates a new time lag equal to 6.3 minutes. A time differential of this magnitude cannot be tolerated due to rapid changes in cumulus clouds during this time span.

The major problem associated with both the initial and latter time lags is the likelihood of rapid formation and dissipation of cumulus clouds during a short time interval. An excellent example

of this is shown in Fig. 6. The selected cumulus cloud as shown in Fig. 6 was traced from whole-sky photos exposed at 5 minute increments on 6 July 1974. Particular notice should be given to the rapid growth during the first 5 minute time span, and again the rapid dissipation during the 15 and 20 minute elapsed times.

It is understood that the latter adjusted position of the whole-sky distribution and its higher correlation may be the result of suitably fitting a random cloud distribution. It is not suggested that the secondary translation of the camera resulted in greater accuracy of camera positioning, but rather to show the need of a synchronized timing system.

Fig. 6 exposes the need of a synchronized timing system when viewing cloud structures from two separate platforms. The lack of synchronization had a pronounced effect upon the transitional nature of the whole-sky coordinate system to fit the S190a time frame, and is believed to have been the major contributing factor to the final analysis.

The point to be made about rapid formation and dissipation of cumulus clouds is that the camera's location for the initial translation may have, in fact, been accurately placed, but due to rapid changes in individual clouds they are no longer identifiable after an elapsed time as short as 90 seconds.

High thin cirrus were also present on the whole-sky photograph resulting in some resolution loss due to scattering of solar radiation. This did not allow well-defined bases for those clouds located in the sun's quadrant. Another disadvantage was most of the cumuli were located in the lower 30° of elevation, thus decreasing their image base size and

increasing measurement errors. In general, image measurement error may be further increased when both cloud and sun are in opposite quadrants and both have low elevation angles, due to alterations in the luminous character of the cloud base.

While this single case study produced less than satisfactory results, this certainly does not discount the invaluable nature of the whole-sky photograph and its useful application to determine spatial positioning of cumulus clouds by providing total sky coverage. The data collection procedure and not the whole-sky camera appears to have accounted for the unsatisfactory analysis.

For the User

A great deal of insight into the photographic system itself was achieved. It is wished to pass some of the knowledge gained to any future user of the whole-sky photograph.

One must attempt to have the photograph center represent, as nearly as possible, the true zenith. Zenith can be easily determined by using a camera tripod with leveling capability.

Once true north is established on the whole-sky print, care must be taken in properly locating the azimuth angles, i.e., the azimuth angles are determined in a counterclockwise fashion while observing the photograph from above (see Fig. 3), as opposed to the normal clockwise procedure.

Knowledge of the magnification factor producing a whole-sky print is required to allow a simple fitting of the transparent overlay. The magnification factor for successive prints should remain constant to avoid alterations in the diameter of the overlay. This is particularly

important for short time-lapse photography.

It is best to use a sun shield (see Lund and Shanklin, 1972) when exposing the photograph negative. Good color contrast, however, can be achieved when a cloud-free sun path exists and a solar shield is neglected during exposure. On the other hand, a thin cirrus deck partially obstructing the solar radiation path may significantly reduce photographic contrast, with or without a shield.

As anticipated, a distinction must be made between the vertical and horizontal extents for a given cloud structure when subjectively determining the dimensions of that cloud from a whole-sky photograph. In contrast to the clouds apparent vertical structure, the image cloud base appears as the darker region. The sun's position relative to the cloud's position largely determines the apparent cloud base, i.e., the apparent image base size is reduced when both sun and cloud have low elevation angles, especially when both are in opposite quadrants. Care must also be taken when dealing with cloud bright spots (see Hulstrom, 1973) and their luminous characteristics.

An extremely important condition for whole-sky photographic analysis is the use of a synchronized timing system, when applicable. The previous analysis suggests that a non-synchronous system may produce large errors due to growth and decay of a cloud structure during specified time intervals. A time-lag introduction requires the translation of at least one coordinate system. The method of translation thus becomes an added analysis factor. The importance of a synchronized timing system cannot be over-emphasized.

As with any fish-eye lens, the user must be aware of its object distortion property and how it affects the analysis procedure. In most

cases, object distortion may be neglected.

Conclusion

The primary meteorological use of the whole-sky photograph has been devoted to determining the probabilities of cloud-free lines-of-sight. Many other practical applications do exist, however, once the geometrical system of the fish-eye lens is fully understood for the type of experiment considered.

Further applications of the fish-eye lens and its whole-sky capability should prove useful in such areas as squall-line dynamical research, fine time-scale studies on growth rates and areal coverages of cumulonimbus structures, outlining areas of localized moisture zones, examination of cloud street phenomena, boundary-layer studies, etc. As previously mentioned, it has been applied to lightning propagation studies, and recently Hulstrom (1973) used the whole-sky photo as an aid in determining cloud bright spots. While the possible uses mentioned above are not exhaustive, they certainly suggest the versatile nature of the whole-sky photograph.

A more objective scheme must be devised when an attempt is made to calculate a cloud's physical dimensions and its spatial location from the whole-sky camera. A computer-oriented grid system is, perhaps, the answer. It is understood, however, that difficulties would still arise in the lower angles of elevation. Stereoscopic analysis of whole-sky photographs should prove useful in error reduction for low-angle elevation measurements as well as for all angles.

ACKNOWLEDGMENTS

This research was conducted under SKYLAB Experiment Project Number-582, Severe Storm Environments by Dr. D. E. Pitts, Dr. Y. K. Sasaki, and Mr. J. T. Lee and under NASA contract NAS 9-13360 with Dr. Y. K. Sasaki of the University of Oklahoma. The Photographic Laboratory of the Earth Observations Division of Johnson Space Center, Houston, Texas, provided the S190a frame enlargement and Mr. J. T. Lee, National Severe Storms Laboratory (NOAA, ERL), Norman, Oklahoma, provided the necessary upper air data. I am grateful for their aid and support in this study. I am deeply indebted to Dr. Y. K. Sasaki who made this study possible through his support and encouragement, and to Dr. M. J. McFarland, University of Oklahoma, for his support and many helpful suggestions. I owe a special thanks to Ms. Anita Cameron for typing this report.

REFERENCES

Hulstrom, R. L., 1973: The cloud bright spot. Photogrammetric Engineering, 39, 370-376.

Krider, E. P., 1974: An unusual photograph of an air lightning discharge. Weather, 29, 24-27.

Lund, I. A., 1973: A model for estimating joint probabilities of cloud-free lines-of-sight through the atmosphere. J. Appl. Meteor., 12, 1040-1043.

_____, 1973: Persistence and recurrence probabilities of cloud-free and cloudy lines-of-sight through the atmosphere. J. Appl. Meteor., 12, 1222-1228.

_____, and M. D. Shanklin, 1972: Photogrammetrically determined cloud-free lines-of-sight through the atmosphere. J. Appl. Meteor., 11, 773-782.

_____, and M. D. Shanklin, 1973: Universal methods for estimating probabilities of cloud-free lines-of-sight through the atmosphere. J. Appl. Meteor., 12, 28-35.

NASA, 1972a: Skylab EREP investigator's data book. Principal Investigator Management Office, Johnson Space Center, Houston, Texas.

NASA, 1974: Summary of flight performance of the Skylab earth resources experiment package (EREP). NASA Johnson Space Center, Houston, Texas, 44 pp.

Pochop, L. O., and M. D. Shanklin, 1966: Sky cover photograms, a new technique. Weatherwise, 19, 198-200.

Rapp, R. R., C. Schultz, and E. Rodrigues, 1973: Cloud-free lines-of-sight calculations. J. Appl. Meteor., 12, 484-493.

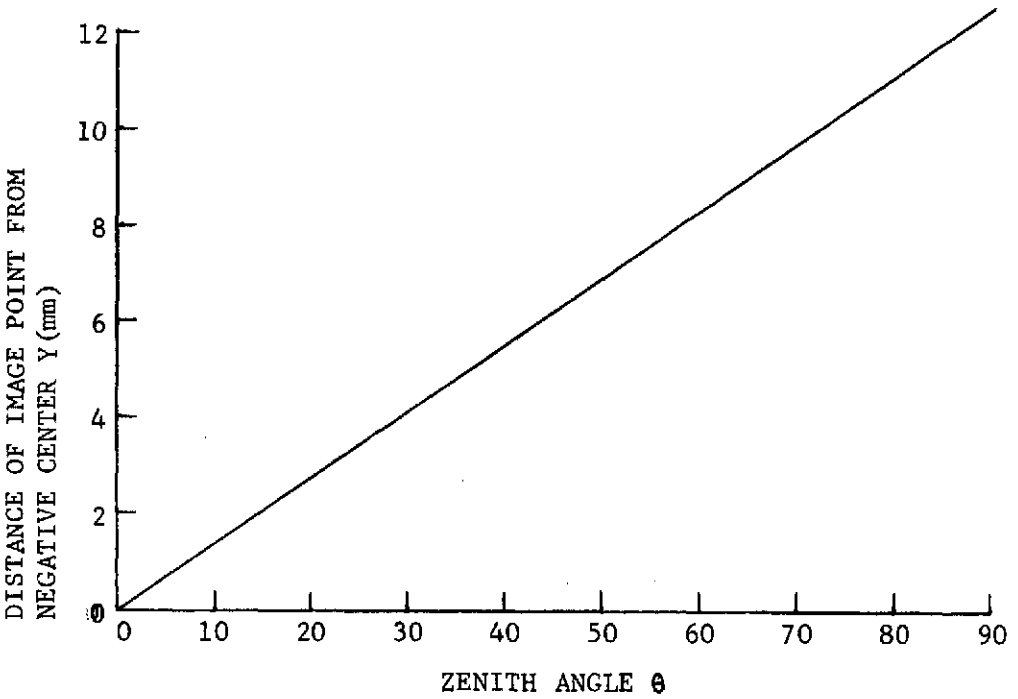

FIG.1. Relationship between the zenith angle and the distance of an image point from the center of the fish-eye lens for the linear projection, $Y=C\theta$. For the type of lens used, the constant C is approximately 0.14 (mm/deg). (after the Fisheye-NIKKOR Auto Manual).

y	$\theta°$	$\Delta\theta°$
0	0.00	
0.5	3.58	3.58
1.0	7.17	3.59
1.5	10.76	3.59
2.0	14.36	3.60
2.5	17.98	3.62
3.0	21.62	3.64
3.5	25.27	3.65
4.0	28.95	3.68
4.5	32.66	3.71
5.0	36.40	3.74
5.5	40.17	3.77
6.0	43.98	3.81
6.5	47.83	3.85
7.0	51.73	3.90
7.5	55.67	3.94
8.0	59.67	4.00
8.5	63.72	4.05
9.0	67.84	4.12
9.5	72.03	4.19
10.0	76.31	4.28
10.5	80.69	4.38
11.0	85.21	4.52
11.5	89.97	4.76

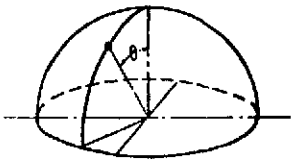

θ: Zenith angle.

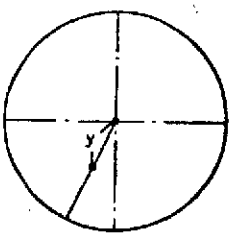

Y: Distance of image point from negative center.

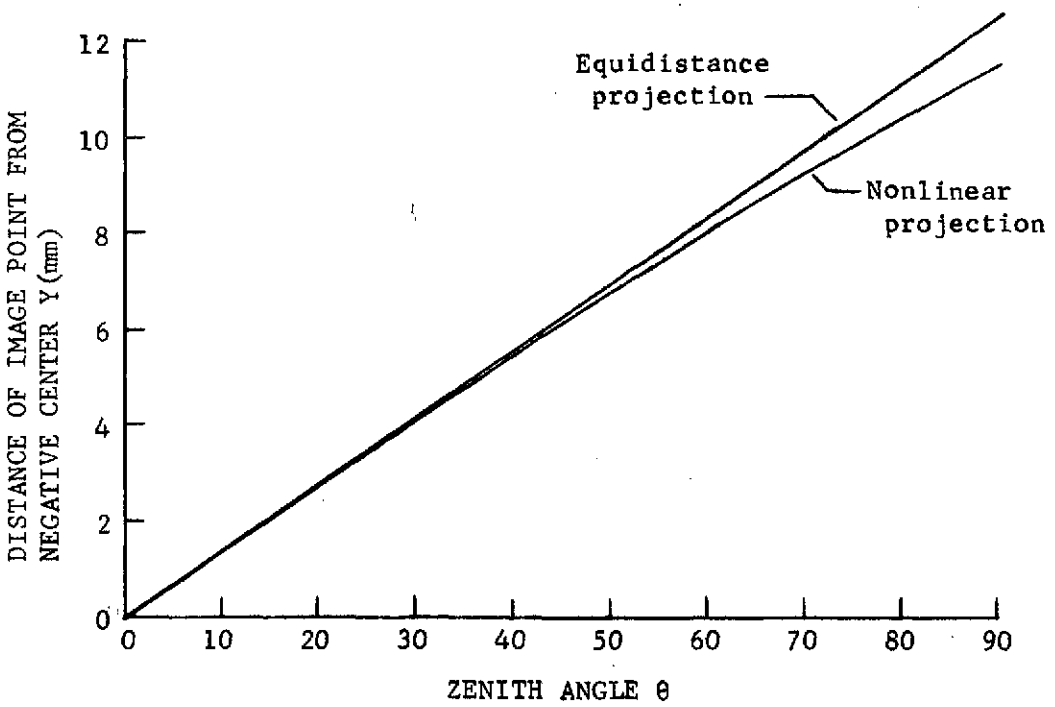

FIG.2. Graphical comparison between the equidistance and nonlinear projection methods. Noticable deviations between the two projections begin near 45 deg. The above table gives the zenith angle and image distance from the negative center for the nonlinear case. (after the Fisheye-NIKKOR Auto Manual).

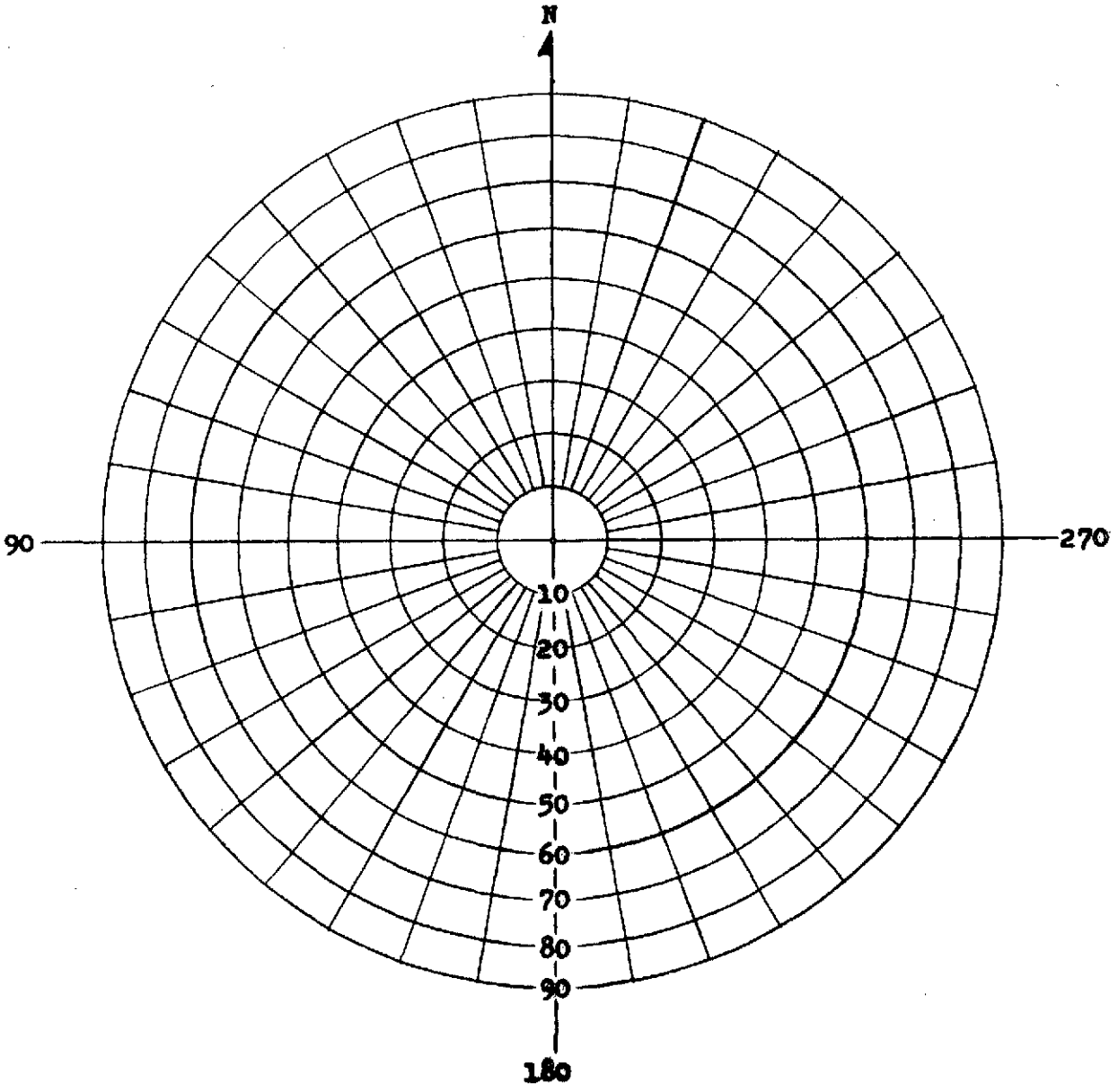

FIG.3. An example of the plastic transparency used to overlay the whole-sky photograph that displays the zenith and principal azimuthal angles. Particular attention should be given to the counterclockwise fashion of the azimuth angles.

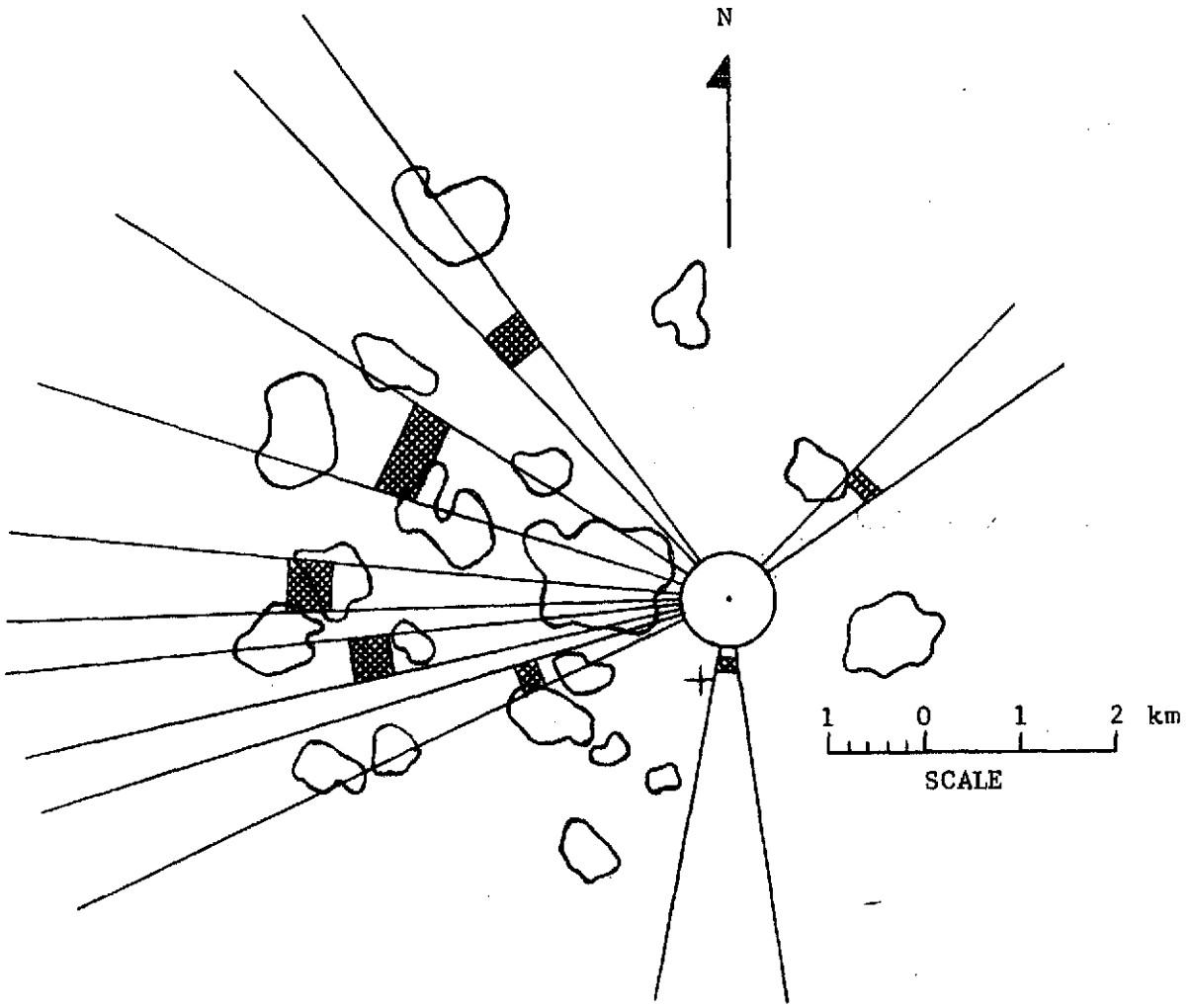

FIG.4. Comparative distributions of the selected cumuli constrained to the camera's initial transitory time of 90 seconds. The hatched areas correspond to the whole-sky distribution along with the field-of-views for the individual cumuli. The " + " symbol represents the camera's position prior to its translation. A poor correlation between the two distributions exists in this case.

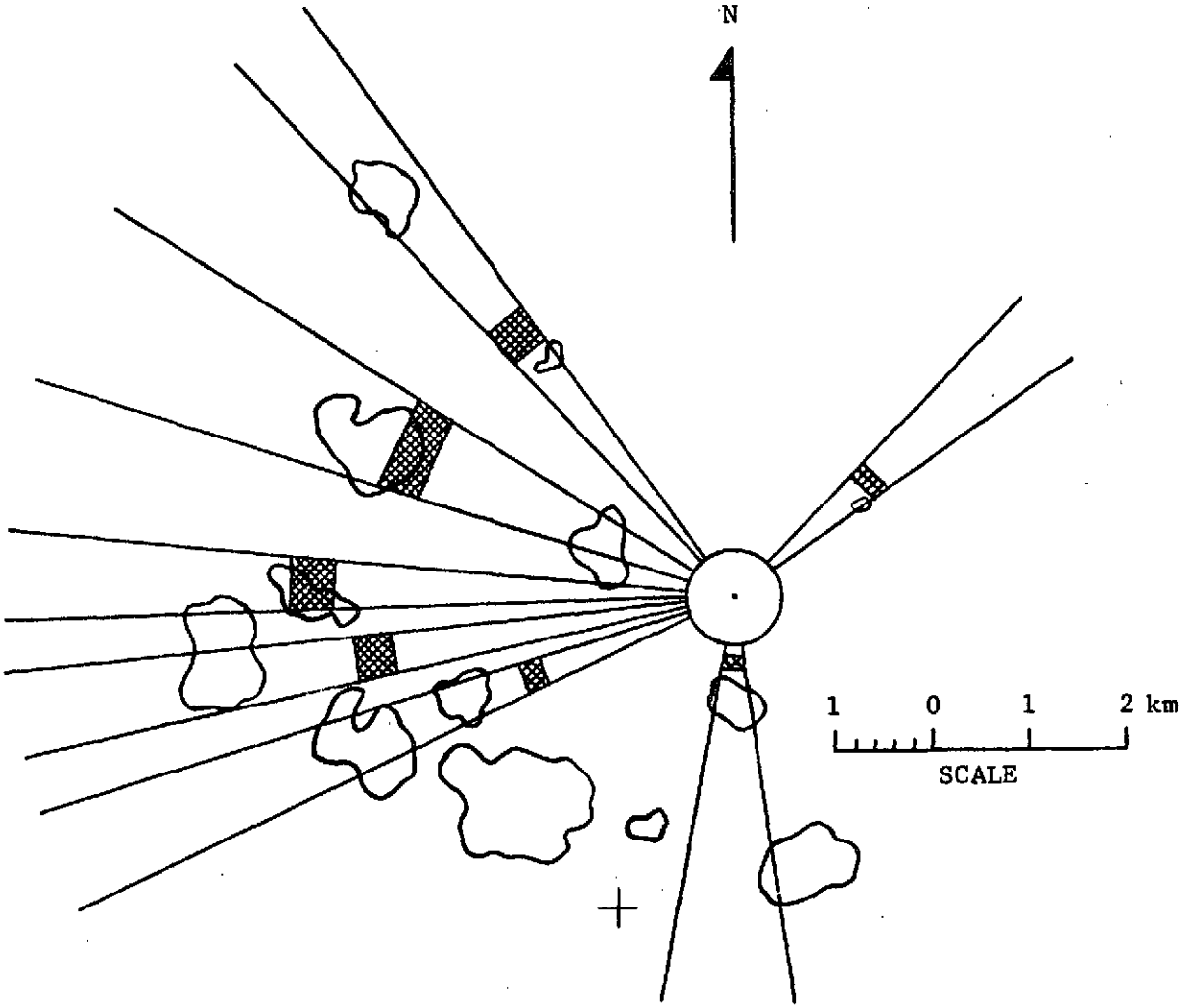

FIG.5. Comparative distributions of the selected cumuli constrained to the camera's secondary transitory time period. The hatched areas correspond to the whole-sky distribution along with the field-of-views for the individual cumuli. The " + " symbol represents the camera's position prior to any translation. A much better correlation exists here than in the previous figure.

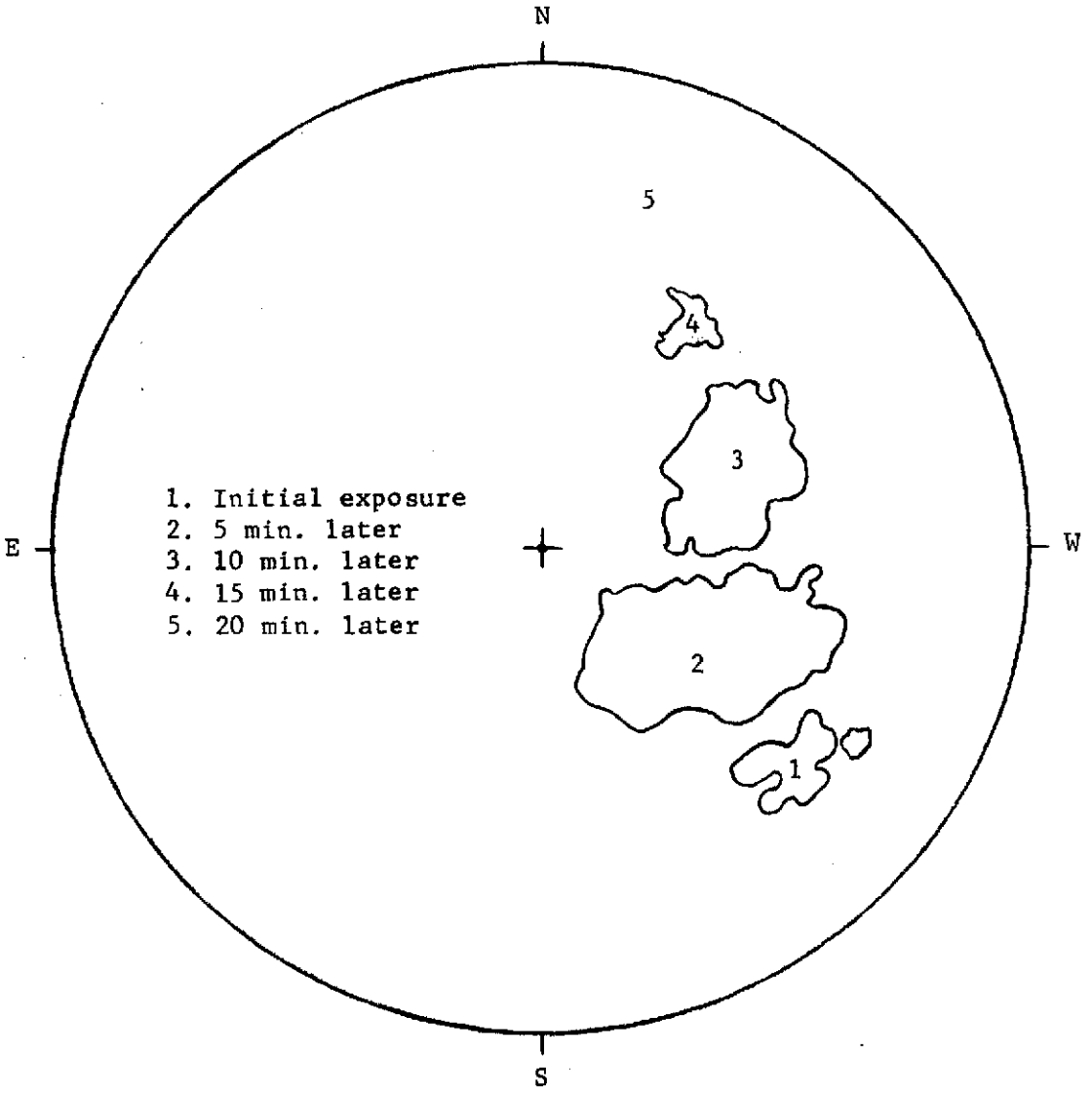

FIG.6. An example showing rapid formation and dissipation characteristics for a single cumulus cloud during short-time exposure intervals of 5 min. Notice that the cloud was non-existant during sky exposure at 5 min. following its #4 position. The cloud was exposed by the whole-sky camera.